tion buffer at 65°C for 12 hours. To remove protein and RNA, samples were incubated with RNaseA for 1 hour at 37°C and proteinase K treatment for 1 hour at 37°C. Samples were purified by PCR purification kit (Qiagen). The amount of DNA immunoprecipitated with HA-tagged protein was quantified by real-time PCR with primers flanking the *Fos* promoter, including the CRE element (forward, 5′-TCCTACACGCGGAAGGTCTAGG-3′; reverse, 5′-TAGAAGCGCTGTGAATGGATGG-3′). Primers 5′-GCACTAATTAGTCGCGGTGGTGG-3′ (forward) and 5′-CAGGGTCTTAGTGGGATCAAGG-3′ (reverse) were used as a negative control.

Accession number. The profiling data cited in Supplemental Figure 6 are available at GEO (accession no. GSE41123).

Statistics. Statistical analyses were carried out using GraphPad Prism (version 5.01; GraphPad Software). Data were analyzed using ANOVA, and *P* values less than 0.05 were considered statistically significant.

Study approval. Animal experiments were approved by the Gifu University Animal Experiment Committee, and the care of the animals was in accordance with institutional guidelines. All clinical samples were approved for analysis by the Ethics Committee at Kyoto University Graduate School and Faculty of Medicine (Kyoto, Japan). Written informed consent was obtained from all patients with cancers analyzed in this study.

Acknowledgments

The authors thank K. Woltjen and T. Yamamoto (CiRA, Kyoto University) for careful reading of the manuscript and helpful comments. We also thank T. Motohashi (Tissue and Organ Development Regeneration and Advanced Medical Science) for helpful discussion and the members of the Department of Orthopedic Surgery and Department of Tumor Pathology, Gifu University Graduate School of Medicine; the Department of Orthopaedic Surgery, Graduate School of Medicine, Kyoto University; and the Toguchida and Yamada laboratories for their valuable technical assistance. This study was supported by grants from the Ministry of Education, Culture, Sports, Science, and Technology of Japan and from the Ministry of Health, Labor, and Welfare of Japan.

Received for publication February 28, 2012, and accepted in revised form November 1, 2012.

Address correspondence to: Yasuhiro Yamada, Center for iPS Cell Research and Application (CiRA), Institute for Integrated Cell-Material Sciences (WPI-iCeMS), Kyoto University, 53 Kawahara-cho, Shogoin, Sakyo-ku, Kyoto 606-8507, Japan. Phone: 81.75.366.7034; Fax: 81.75.366.7093; E-mail: y-yamada@cira.kyoto-u.ac.jp. Or to: Takatoshi Ohno, Department of Orthopaedic Surgery, Gifu University Graduate School of Medicine, 1-1 Yanagido, Gifu 501-1194, Japan. Phone: 81.58.230.6333; Fax: 81.58.230.6334; E-mail: takaohno@gifu-u.ac.jp.

1. Enzinger FM. Clear-cell sarcoma of tendons and aponeuroses. An analysis of 21 cases. *Cancer.* 1965; 18:1163–1174.
2. Covinsky M, Gong S, Rajaram V, Perry A, Pfeifer J. EWS-ATF1 fusion transcripts in gastrointestinal tumors previously diagnosed as malignant melanoma. *Hum Pathol.* 2005;36(1):74–81.
3. Deenik W, Mooi WJ, Rutgers EJ, Peterse JL, Hart AA, Kroon BB. Clear cell sarcoma (malignant melanoma) of soft parts: A clinicopathologic study of 30 cases. *Cancer.* 1999;86(6):969–975.
4. Ferrari A, et al. Clear cell sarcoma of tendons and aponeuroses in pediatric patients: a report from the Italian and German Soft Tissue Sarcoma Cooperative Group. *Cancer.* 2002;94(12):3269–3276.
5. Finley JW, Hanypsiak B, McGrath B, Kraybill W, Gibbs JF. Clear cell sarcoma: the Roswell Park experience. *J Surg Oncol.* 2001;77(1):16–20.
6. Eckardt JJ, Pritchard DJ, Soule EH. Clear cell sarcoma. A clinicopathologic study of 27 cases. *Cancer.* 1983;52(8):1482–1488.
7. Kawai A, et al. Clear cell sarcoma of tendons and aponeuroses: a study of 75 patients. *Cancer.* 2007;109(1):109–116.
8. Kindblom LG, Lodding P, Angervall L. Clear-cell sarcoma of tendons and aponeuroses. An immunohistochemical and electron microscopic analysis indicating neural crest origin. *Virchows Arch A Pathol Anat Histopathol.* 1983;401(1):109–128.
9. Segal NH, et al. Classification of clear-cell sarcoma as a subtype of melanoma by genomic profiling. *J Clin Oncol.* 2003;21(9):1775–1781.
10. Bridge JA, Borek DA, Neff JR, Huntrakoon M. Chromosomal abnormalities in clear cell sarcoma. Implications for histogenesis. *Am J Clin Pathol.* 1990; 93(1):26–31.
11. Bridge JA, Sreekantaiah C, Neff JR, Sandberg AA. Cytogenetic findings in clear cell sarcoma of tendons and aponeuroses. Malignant melanoma of soft parts. *Cancer Genet Cytogenet.* 1991;52(1):101–106.
12. Sandberg AA, Bridge JA. Updates on the cytogenetics and molecular genetics of bone and soft tissue tumors: clear cell sarcoma (malignant melanoma of soft parts). *Cancer Genet Cytogenet.* 2001;130(1):1–7.
13. Kim J, Lee K, Pelletier J. The DNA binding domains of the WT1 tumor suppressor gene product and chimeric EWS/WT1 oncoprotein are functionally distinct. *Oncogene.* 1998;16(8):1021–1030.
14. Lessnick SL, Braun BS, Denny CT, May WA. Multiple domains mediate transformation by the Ewing's sarcoma EWS/FLI-1 fusion gene. *Oncogene.* 1995;10(3):423–431.
15. Pan S, Ming KY, Dunn TA, Li KK, Lee KA. The EWS/ATF1 fusion protein contains a dispersed activation domain that functions directly. *Oncogene.* 1998;16(12):1625–1631.
16. Ohno T, Ouchida M, Lee L, Gatalica Z, Rao VN, Reddy ES. The EWS gene, involved in Ewing family of tumors, malignant melanoma of soft parts and desmoplastic small round cell tumors, codes for an RNA binding protein with novel regulatory domains. *Oncogene.* 1994;9(10):3087–3097.
17. Petermann R, Mossier BM, Aryee DN, Khazak V, Golemis EA, Kovar H. Oncogenic EWS-Fli1 interacts with hsRPB7, a subunit of human RNA polymerase II. *Oncogene.* 1998;17(5):603–610.
18. Gonzalez GA, Montminy MR. Cyclic AMP stimulates somatostatin gene transcription by phosphorylation of CREB at serine 133. *Cell.* 1989;59(4):675–680.
19. Comb M, Birnberg NC, Seasholtz A, Herbert E, Goodman HM. A cyclic AMP- and phorbol ester-inducible DNA element. *Nature.* 1986; 323(6086):353–356.
20. Montminy MR, Sevarino KA, Wagner JA, Mandel G, Goodman RH. Identification of a cyclic-AMP-responsive element within the rat somatostatin gene. *Proc Natl Acad Sci U S A.* 1986;83(18):6682–6686.
21. Li KK, Lee KA. MMSP tumor cells expressing the EWS/ATF1 oncogene do not support cAMP-inducible transcription. *Oncogene.* 1998;16(10):1325–1331.
22. Brown AD, Lopez-Terrada D, Denny C, Lee KA. Promoters containing ATF-binding sites are de-regulated in cells that express the EWS/ATF1 oncogene. *Oncogene.* 1995;10(9):1749–1756.
23. Fujimura Y, Ohno T, Siddique H, Lee L, Rao VN, Reddy ES. The EWS-ATF-1 gene involved in malignant melanoma of soft parts with t(12;22) chromosome translocation, encodes a constitutive transcriptional activator. *Oncogene.* 1996;12(1):159–167.
24. Jishage M, Fujino T, Yamazaki Y, Kuroda H, Nakamura T. Identification of target genes for EWS/ATF-1 chimeric transcription factor. *Oncogene.* 2003; 22(1):41–49.
25. Davis IJ, et al. Oncogenic MITF dysregulation in clear cell sarcoma: defining the MiT family of human cancers. *Cancer Cell.* 2006;9(6):473–484.
26. Antonescu CR, Tschernyavsky SJ, Woodruff JM, Jungbluth AA, Brennan MF, Ladanyi M. Molecular diagnosis of clear cell sarcoma: detection of EWS-ATF1 and MITF-M transcripts and histopathological and ultrastructural analysis of 12 cases. *J Mol Diagn.* 2002;4(1):44–52.
27. Granter SR, Weilbaecher KN, Quigley C, Fletcher CD, Fisher DE. Clear cell sarcoma shows immunoreactivity for microphthalmia transcription factor: further evidence for melanocytic differentiation. *Mod Pathol.* 2001;14(1):6–9.
28. Li KK, et al. The melanocyte inducing factor MITF is stably expressed in cell lines from human clear cell sarcoma. *Br J Cancer.* 2003;89(6):1072–1078.
29. Levy C, Khaled M, Fisher DE. MITF: master regulator of melanocyte development and melanoma oncogene. *Trends Mol Med.* 2006;12(9):406–414.
30. Garraway LA, et al. Integrative genomic analyses identify MITF as a lineage survival oncogene amplified in malignant melanoma. *Nature.* 2005; 436(7047):117–122.
31. Speleman F, Delattre O, Peter M, Hauben E, Van Roy N, Van Marck E. Malignant melanoma of the soft parts (clear-cell sarcoma): confirmation of EWS and ATF-1 gene fusion caused by a t(12;22) translocation. *Mod Pathol.* 1997;10(5):496–499.
32. Jiang X, Rowitch DH, Soriano P, McMahon AP, Sucov HM. Fate of the mammalian cardiac neural crest. *Development.* 2000;127(8):1607–1616.
33. Seternes OM, Sorensen R, Johansen B, Loennechen T, Aarbakke J, Moens U. Synergistic increase in c-fos expression by simultaneous activation of the ras/raf/map kinase- and protein kinase A signaling pathways is mediated by the c-fos AP-1 and SRE sites. *Biochim Biophys Acta.* 1998;1395(3):345–360.
34. Ginty DD, Bonni A, Greenberg ME. Nerve growth factor activates a Ras-dependent protein kinase that stimulates c-fos transcription via phosphorylation of CREB. *Cell.* 1994;77(5):713–725.
35. Sassone-Corsi P, Visvader J, Ferland L, Mellon PL, Verma IM. Induction of proto-oncogene fos transcription through the adenylate cyclase pathway:

characterization of a cAMP-responsive element. *Genes Dev.* 1988;2(12A):1529–1538.
36. Weinstein IB. Cancer. Addiction to oncogenes – the Achilles heal of cancer. *Science.* 2002;297(5578):63–64.
37. Beard C, Hochedlinger K, Plath K, Wutz A, Jaenisch R. Efficient method to generate single-copy transgenic mice by site-specific integration in embryonic stem cells. *Genesis.* 2006;44(1):23–28.
38. Hochedlinger K, Yamada Y, Beard C, Jaenisch R. Ectopic expression of Oct-4 blocks progenitor-cell differentiation and causes dysplasia in epithelial tissues. *Cell.* 2005;121(3):465–477.
39. Haldar M, Hancock JD, Coffin CM, Lessnick SL, Capecchi MR. A conditional mouse model of synovial sarcoma: insights into a myogenic origin. *Cancer Cell.* 2007;11(4):375–388.
40. Riggi N, et al. Development of Ewing's sarcoma from primary bone marrow-derived mesenchymal progenitor cells. *Cancer Res.* 2005;65(24):11459–11468.
41. Adameyko I, et al. Schwann cell precursors from nerve innervation are a cellular origin of melanocytes in skin. *Cell.* 2009;139(2):366–379.
42. Guller M, et al. c-Fos overexpression increases the proliferation of human hepatocytes by stabilizing nuclear Cyclin D1. *World J Gastroenterol.* 2008; 14(41):6339–6346.
43. Pandey MK, Liu G, Cooper TK, Mulder KM. Knockdown of c-Fos suppresses the growth of human colon carcinoma cells in athymic mice. *Int J Cancer.* 2012;130(1):213–222.
44. Saez E, et al. c-fos is required for malignant progression of skin tumors. *Cell.* 1995;82(5):721–732.
45. Grigoriadis AE, Schellander K, Wang ZQ, Wagner EF. Osteoblasts are target cells for transformation in c-fos transgenic mice. *J Cell Biol.* 1993; 122(3):685–701.
46. Wang ZQ, Grigoriadis AE, Mohle-Steinlein U, Wagner EF. A novel target cell for c-fos-induced oncogenesis: development of chondrogenic tumours in embryonic stem cell chimeras. *EMBO J.* 1991;10(9):2437–2450.
47. Nozawa S, et al. Inhibition of platelet-derived growth factor-induced cell growth signaling by a short interfering RNA for EWS-Fli1 via down-regulation of phospholipase D2 in Ewing sarcoma cells. *J Biol Chem.* 2005;280(30):27544–27551.
48. Yamamoto T, et al. Simultaneous inhibition of mitogen-activated protein kinase and phosphatidylinositol 3-kinase pathways augment the sensitivity to actinomycin D in Ewing sarcoma. *J Cancer Res Clin Oncol.* 2009;135(8):1125–1136.
49. Moritake H, et al. Newly established clear cell sarcoma (malignant melanoma of soft parts) cell line expressing melanoma-associated Melan-A antigen and overexpressing C-MYC oncogene. *Cancer Genet Cytogenet.* 2002;135(1):48–56.
50. Chai Y, et al. Fate of the mammalian cranial neural crest during tooth and mandibular morphogenesis. *Development.* 2000;127(8):1671–1679.
51. Yamauchi Y, et al. A novel transgenic technique that allows specific marking of the neural crest cell lineage in mice. *Dev Biol.* 1999;212(1):191–203.
52. Sakai K, Miyazaki J. A transgenic mouse line that retains Cre recombinase activity in mature oocytes irrespective of the cre transgene transmission. *Biochem Biophys Res Commun.* 1997;237(2):318–324.
53. Srinivas S, et al. Cre reporter strains produced by targeted insertion of EYFP and ECFP into the ROSA26 locus. *BMC Dev Biol.* 2001;1:4.

Ann Surg Oncol (2012) 19:S539–S548
DOI 10.1245/s10434-011-2040-5

Annals of
SURGICAL ONCOLOGY
OFFICIAL JOURNAL OF THE SOCIETY OF SURGICAL ONCOLOGY

ORIGINAL ARTICLE – TRANSLATIONAL RESEARCH AND BIOMARKERS

Increased CD13 Expression Reduces Reactive Oxygen Species, Promoting Survival of Liver Cancer Stem Cells via an Epithelial–Mesenchymal Transition-like Phenomenon

Ho Min Kim[1], Naotsugu Haraguchi[1], Hideshi Ishii[1,2], Masahisa Ohkuma[1,3], Miho Okano[1], Koshi Mimori[2], Hidetoshi Eguchi[1], Hirofumi Yamamoto[1], Hiroaki Nagano[1], Mitsugu Sekimoto[1], Yuichiro Doki[1], and Masaki Mori[1]

[1]Department of Gastroenterological Surgery, Osaka University Graduate School of Medicine, Osaka, Japan; [2]Department of Molecular and Cellular Biology, Division of Molecular and Surgical Oncology, Kyushu University, Medical Institute of Bioregulation, Beppu, Ohita, Japan; [3]Department of Gastroenterological Surgery, Jikei Collage Graduate School of Medicine, Tokyo, Japan

ABSTRACT

Background. Recently, it has been reported that a small population of cancer stem cells (CSCs) play a role in resistance to chemotherapy and radiation therapy. We reported that $CD13^+$ liver CSCs survive in hypoxic lesions after chemotherapy, presumably through increased expression of CD13/Aminopeptidase N, which is a scavenger enzyme in the reactive oxygen species (ROS) metabolic pathway. On the other hand, the concept of epithelial–mesenchymal transition (EMT) was indicated by a recent study showing an increased plasticity linked to the cellular "stemness" of CSCs.

Methods. To study the relationship between CSCs and EMT, we examined biological characteristics of liver cancer cell lines with EMT by exposing transforming growth factor-β (TGF-β).

Results. We showed that a TGF-β-induced EMT-like phenomenon is associated with increased CD13 expression in liver cancer cells. This phenomenon prevents further increases in the ROS level as well as the induction of apoptosis, promoting the survival of $CD13^+$ CSCs, whereas inhibition of CD13 stimulates apoptosis. Immunohistochemical analysis also indicated that after chemotherapy, CD13 was coexpressed with N-cadherin in surviving cancer cells within fibrous capsules. We have demonstrated that CD13 expression plays a role in supporting the survival of CSCs and that there is an EMT-associated reduction in ROS elevation.

Conclusions. This novel and consistent linkage between functional CSC markers and the EMT phenomenon suggests a bona fide candidate for targeted therapy for EMT-mediated invasion and metastasis of liver cancer.

Cancer stem cells (CSCs) are believed to share unique characters with normal stem cells, self-renewal ability, and produce differentiated cells.[1,2] Additionally, CSCs play a key role in resistance to chemotherapy and radiotherapy. CSCs give rise to cancer recurrence even though most cancer cells have been disrupted after this therapy.[3] Since the identification of CSCs in leukemia,[4–6] CSCs have been reported in various solid tumors; brain, head and neck, breast, and colon.[7–12]

In studies of hepatocellular carcinoma, side population (SP) fraction, CD133, CD90, CD44, and epithelial cell adhesion molecules (EpCAMs) were reported as markers of CSCs or cancer-/tumor-initiating cells.[13–20] We have reported CD13 as a novel liver CSCs marker and as candidate therapeutic target with some sets of functional analyses.[21] We showed that CD13+ cells mainly existed in SP fraction, contained potentially dye-long retaining cell, and had high tumorigenic activity. Additionally, CD13 + CSCs showed strong chemoradiation resistance in vitro and in vivo, by protecting cells from DNA damage via regulation of the

Electronic supplementary material The online version of this article (doi:10.1245/s10434-011-2040-5) contains supplementary material, which is available to authorized users.

First Received: 14 March 2011;
Published Online: 31 August 2011

H. Ishii
e-mail: hishii@cfs.med.osaka-u.ac.jp

M. Mori
e-mail: mmori@gesurg.med.osaka-u.ac.jp

reactive oxygen species (ROS) level. Inhibition of CD13-induced tumor cell apoptosis resulted in tumor disruption via blocking self-renewal activity. CD13 also has been associated with tumor invasion, regulation of angiogenesis, and resistance to apoptosis.[22–24]

Epithelial–mesenchymal transition (EMT) plays crucial roles in developmental processes, such as neural crest and mesoderm formation during embryogenesis, and has been focused as a key process in tumor invasion, metastasis, and tumorigenicity.[25,26] EMT has been well characterized by numerous pathways of transcriptional factors, including Snail, Twist, and Zeb, which are generally promoted by transforming growth factor (TGF) β superfamily.[25] In the study of mammary epithelial cells, it was reported that EMT generates normal mammary epithelial cells with properties of stem cells.[27] In the study of breast cancer CSCs, it has reported that breast cancer cells increase malignant potential with increased CSCs phenotype by the treatment of EMT inducers.[27] Furthermore, ROS have been proposed recently to be involved in tumor metastasis, which is a complicated process, including EMT of cancer cells and the microenvironment inside or around the tumor lesion.[28,29]

In the present study, we identify a TGF-β-induced EMT-like phenomenon is associated with increased CD13 expression in liver cancer cells and plays a role in the reduction of the intracellular ROS level, promoting the survival of liver CSCs. The present data indicate a novel and consistent linkage between CD13, a functional CSC marker, and the EMT phenomenon.

MATERIALS AND METHODS

Cell Culture

Human hepatocellular carcinoma (HCC) cells, HuH7, and PLC/PRF/5, obtained from the Cell Resource Center for Biomedical Research, Institute of Development, Aging, and Cancer (Tohoku University, Sendai, Japan) were cultured in an RPMI 1640 medium (Invitrogen) with 10% fetal bovine serum (FBS; GIBCO). Cells were cultured at 37°C in a humidified atmosphere containing 5% CO_2.

Induction and Reversal of EMT

Cells were seeded and incubated in a standard medium for 48 h and then incubated in a serum-free medium supplemented with 5 μg/ml insulin and 10 ng/ml endothelial growth factor at 37°C in an atmosphere containing 5% CO_2 for 48–72 hr with TGF-β1 (R&D) at concentrations of 0–5 ng/ml with daily replacement of the fresh culture medium.[30]

Gene Expression Study

Total RNA was prepared using TRIzol reagent (Invitrogen). Reverse transcription was performed with SuperScriptIII (Invitrogen). Quantitative real-time (qRT)-PCR was performed using a Light Cycler TaqMan Master kit (Roche Diagnostics). The expression of mRNA copies was normalized against glyceraldehyde-3-phosphate dehydrogenase (GAPDH) mRNA expression. The PCR primers used for amplification were as follows: GAPDH, 5′-GTCAACGGATTTGGTC TGTATT-3′ (forward) and 5′-AGTCTTCTGGGTGGCAGT-GAT-3′ (reverse); N-cadherin, 5′-ACAGTGGCCACCTA CAAAGG-3′ (forward) and 5′-CCGAGATGGGGTTGA TAATG-3′ (reverse); fibronectin, 5′-CAGTGGGAGACCTC GAGAAG-3′ (forward) and 5′-TCCCTCGGAACATCA GAAAC-3′ (reverse); vimentin, 5′-GAGTCCACTGAGTAC CGGAGAC-3′ (forward) and 5′-TGTAGGTGGCAATCT CAATGTC-3′ (reverse); E-cadherin, 5′-ACACCATCCTCAG CCAAGA-3′ (forward) and 5′-CGTAGGGAAACTCTCT CGGT-3′ (reverse); Bmi-1, 5′-TGTAAAACGTGTATTGTT CGTTAC-3′ (forward) and 5′-CAATATCTTGGAGAGTT TTATCTGACC-3′ (reverse); Notch-1, 5′-CGCACAAG GTGTCTTCCAG-3′ (forward) and 5′-AGGATCAGTGG CGTCGTG-3′ (reverse); Gclm, 5′-GAAGAAGATATTTT TCCTGTCATTGAT-3′ (forward) and 5′-CCATTCATG TATTGAAGAGTGAATTT-3′ (reverse); Gss, 5′-CCTGCTA GTGGATGCTGTCA-3′ (forward) and 5′-TCATCCTGTTT GATGGTGCT-3′ (reverse); c-Maf, 5′-AATACGAGAAGC TGGTGAGCAA-3′ (forward) and 5′-CGGGAGAGGAAGG GTTGTC-3′ (reverse).

Flow Cytometric Analysis and Cell Sorting

The following antibodies were used to characterize cancer cells: allophycocyanin (APC)-conjugated anti-human CD133/1 (clone AC133, Miltenyi-Biotec), APC-conjugated anti-human CD90 (clone 5E10, BioLegend), APC-conjugated anti-human CD13 (clone WM-15, eBioscience), APC-conjugated anti-human CD324 (E-cadherin, clone 67A4, Bio Legend), phycoerythrin (PE)-conjugated anti-human CD90 (BioLegend), PE-conjugated anti-human CD325 (N-cadherin, clone 8C11, eBioscience), and fluorescein isothiocyanate-conjugated anti-human CD13 (eBioscience).

Dissociated cells were stained with anti-human CD13 with N-cadherin. The labeled cells were analyzed and sorted by the BD FACSAria II Cell Sorter System (Becton Dickinson), and the data were analyzed with Diva software (Becton Dickinson).

Colony Formation Assay

Cells were plated in soft agar at a density of 1×10^3–1×10^4 cells/3.5-cm dish. The base layer was 0.6% agar in the RPMI 1640 medium and the top was 0.2%. Cells were incubated for 30 days; colonies were stained with Diff-Quik kit (Sysmex).

Transplantation of Cancer Cells into Nonobese Diabetic/Severe Combined Immunodeficient (NOD/SCID) Mice

Isolated cells were resuspended in 50 μl of PBS after sorting, and cell aliquots were diluted 1:1 with Growth Factor Reduced Matrigel Matrix (BD Biosciences) and injected subcutaneously into the flank of nonobese diabetic/severe combined immunodeficient (NOD/SCID) mice at densities of 5×10^2, 2.5×10^3, and 1×10^4 cells under anesthesia. After 15 weeks, all tumors were removed and analyzed. All of the animal studies were approved by ethics board of animal study of Osaka University.

ROS Assay

The ROS assay was performed as described previously.[21] Cells were loaded with 10 μM of 2′,7′-dichlorofluorescein diacetate (DCF-DA) at 37°C for 30 min, and cells were pretreated with 100–500 μg/ml of ubenimex (Nihon Kayaku) at 37°C for 24 h and stained with DCF-DA. To evaluate the effect of ROS to induce EMT, 0 to 10 μM of *N*-acetyl cysteine (NAC) (Wako Pure Chemical Industries), which has been known as a general antioxidant agent and ROS inhibitor, was added with or without TGF-β1.

Immunohistochemistry

Ten, fresh, HCC, surgical tissue specimens were obtained from Osaka University, Japan, with the patients' informed consent and the approval of the Research Ethics Board of Osaka University. The VECTASTAIN Elite ABC Kit (Vector Laboratories) was used to detect signals from the antigen-antibody reactions. The primary anti-CD13 mouse polyclonal antibody (38C12; Neomarkers Laboratory Vision) and the primary anti-N-cadherin rabbit polyclonal antibody (YS; Immuno-Biological Laboratories) were used.

Statistical Analysis

Statistical analyses were performed using JMP 8.0.1 for Windows (SAS Institute). Possible differences between groups were analyzed using Student's *t* test, χ^2 test, or Wilcoxon test. A probability level of 0.05 was chosen to indicate statistical significance.

RESULTS

TGF-β-Induced EMT Phenotypes in Liver Cancer Cells

To determine whether liver cancer cells (HuH7, PLC/PRF/5) induced the EMT phenotype, we exposed liver cancer cells to TGF-β. Culturing the liver cancer cells with TGF-β changed their phenotype to spindle-shape morphology (Fig. 1a); this cell phenotype was detected at levels higher than 0.5 ng/ml for HuH7 and 1 ng/ml for PLC/PRF/5. An expression study using qRT-PCR indicated that the mesenchymal markers N-cadherin, fibronectin, and vimentin also were significantly elevated (Fig. 1b). FACS analysis showed that expression of the epithelial marker E-cadherin was decreased (Fig. 1c).

Induced EMT Associated with Increased CD13 Expression in Liver Cancer Cells

To assess whether TGF-β-induced EMT phenotype associate to liver cancer stem cell markers, HuH7 and PLC/PRF/5 cells were incubated with or without TGF-β. By the treatment of TGF-β, expression of CD133 and CD90 was not changed in both HuH7 and PLC/PRF/5.[15–19] In contrast, expression of CD13 was increased almost double in both HuH7 and PLC/PRF/5 (Fig. 2a).[21] Multicolor analysis of N-cadherin and CD13 revealed that N-cadherin$^+$ cells were localized in CD13$^+$ cell fraction (Fig. 2b). Because the CD13 fraction was <3% in HuH7 and >30% in PLC/PRF/5 cells under standard conditions, we used PLC cells in the subsequent studies.

Tumorigenicity of TGF-β-Induced CD13$^+$ Cells

To investigate colony formation ability, the soft agar assay was performed in CD13$^+$/N-cadherin$^-$, CD13$^+$/N-cadherin$^+$, and CD13$^-$/N-cadherin$^-$ cell fractions. The number of CD13$^-$/N-cadherin$^+$ cells was not sufficient for analysis. The soft agar assay showed that after TGF-β stimulation, CD13$^+$/N-cadherin$^-$, and CD13$^+$/N-cadherin$^+$ cells revealed significantly higher colony-forming ability compared with CD13$^-$/N-cadherin$^-$ cells ($P < 0.001$; Fig. 3a and b). There was no appreciable difference between N-cadherin$^+$ and N-cadherin$^-$ cells, which indicated that CD13$^+$ cells exhibited significantly higher colony-forming ability than CD13$^-$ cells. To investigate tumorigenic activity of CD13$^+$/N-cadherin$^-$, CD13$^+$/N-cadherin$^+$, and CD13$^-$/N-cadherin$^-$ cells, isolated 5×10^2, 2.5×10^3, and 1×10^4 cells of each fraction were inoculated into NOD-SCID mice. Serial transplantation experiment indicated that CD13$^+$/N-cadherin$^-$ cells possess higher tumorigenic activity compared with CD13$^-$/N-cadherin$^-$ cells. CD13$^+$/N-cadherin$^+$ cells formed tumor

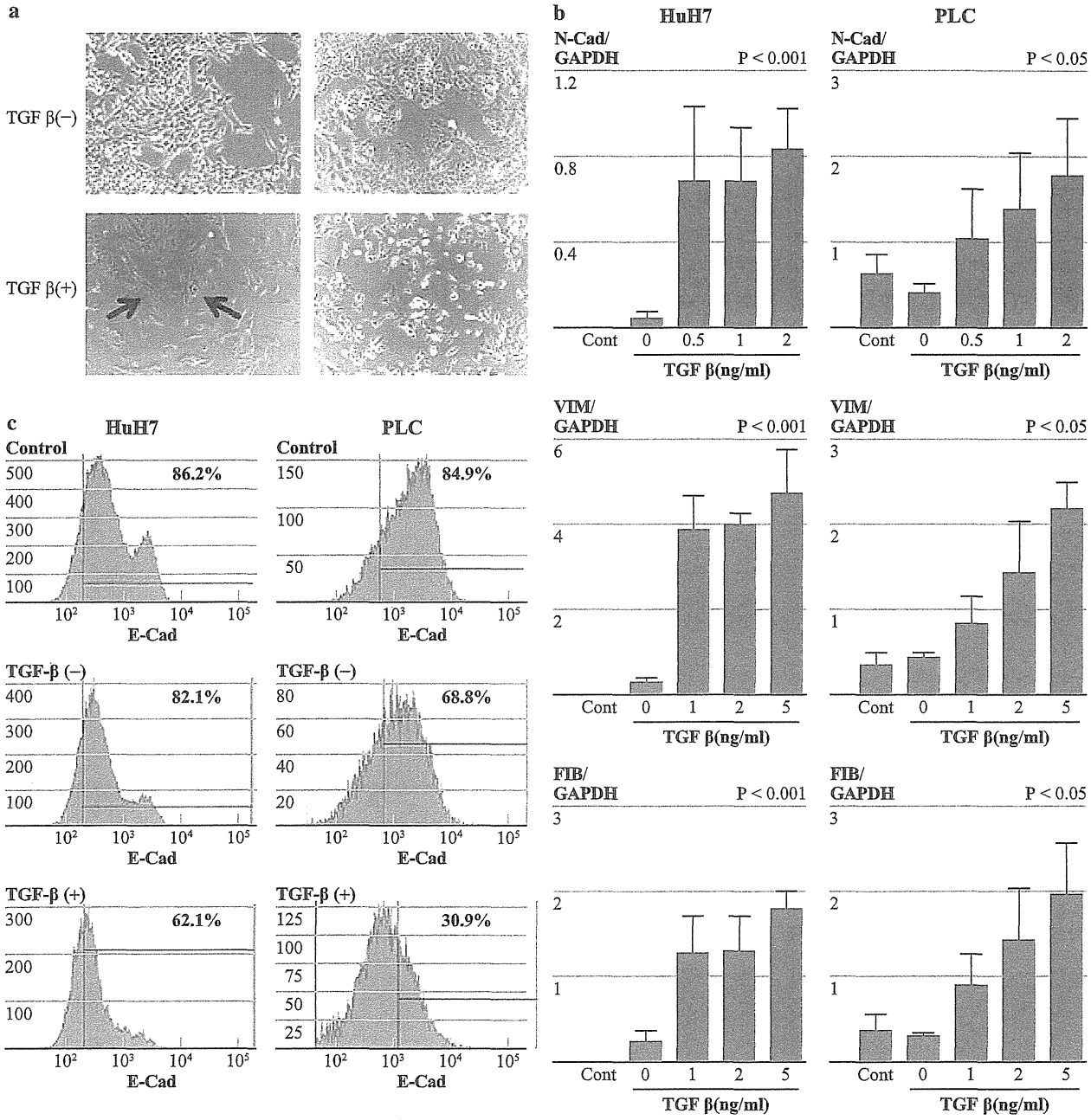

FIG. 1 TGF-β induces EMT in liver cancer cells. **a** Phase contrast microscopy of TGF-β treated (+) or untreated (−) cells of HuH7 and PLC/PRF/5 (PLC). The black arrow shows morphologically spindle-shaped cells. **b** Expression analysis of N-cadherin (N-cad), vimentin (VIM), and fibronectin (FIB) by qRT-PCR. GAPDH was used as internal control. **c** FACS analysis of E-cadherin with or without TGF-β treatment. Control: cells were cultured in conditional medium containing with 10% FBS. TGF-β: cells were treated with (+) or without (−) TGF-β in serum-free medium. HuH7 cells: treated with 1 ng/ml of TGF-β. PLC cells: treated with 2 ng/ml of TGF-β

from 2.5×10^3 cells, which indicated that $CD13^+$/N-cadherin$^+$ cells possess higher tumorigenic activity than $CD13^-$/N-cadherin$^-$ cells but lesser than that of $CD13^+$/N-cadherin$^-$ (Fig. 3c and d). The data are compatible with the results of the in vitro soft agar assay (Fig. 3a and b).

TGF-β Increased the ROS Level in N-cadherin$^+$ Liver Cancer Cells

It has been reported that the control of ROS is indispensable for hematopoietic stem cell maintenance.[31,32] In cancer, low ROS levels and radiation-resistance in breast

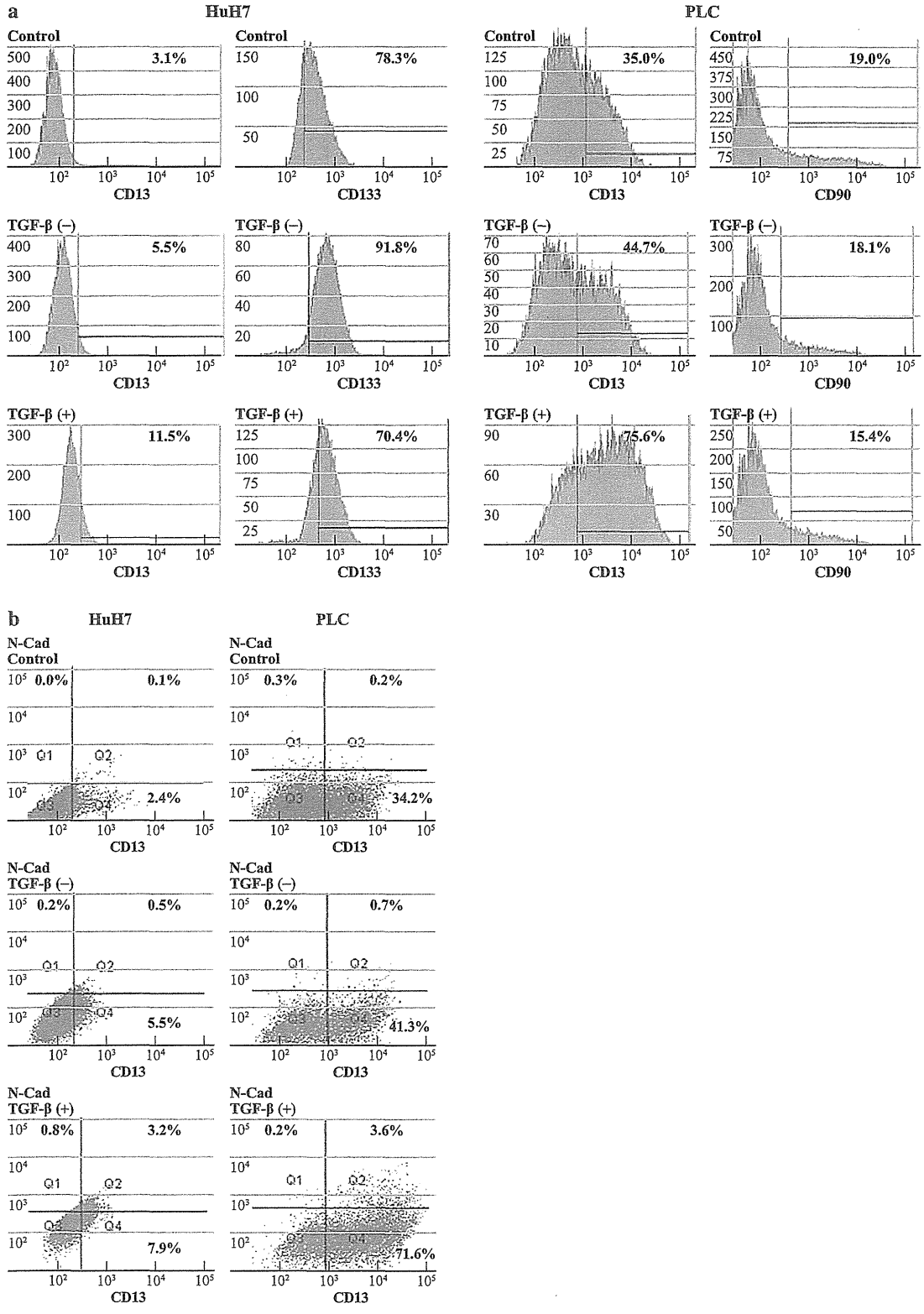

FIG. 2 TGF-β-induced EMT is associated with increased CD13 expression. **a** Expression of CD13 and CD133 in HuH7 cells (*upper*), and CD13 and CD90 in PLC cells (*lower*). *Each number* shows percentage of positive fraction of each marker. HuH7 cells: treated with 1 ng/ml of TGF-β. PLC cells: treated with 2 ng/ml of TGF-β. Control: cells were cultured in conditional medium containing with 10% FBS. **b** Expression analysis of N-cadherin (N-cad) and CD13 with or without TGF-β treatment

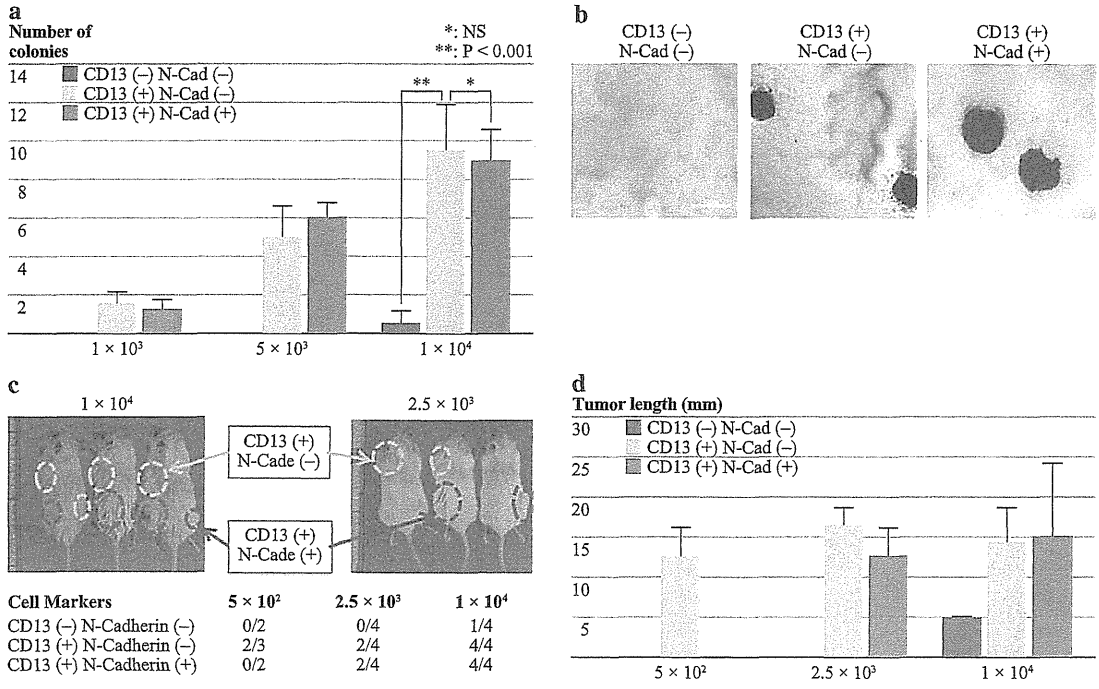

FIG. 3 $CD13^+$ liver cancer cells have higher tumorigenicity than $CD13^-$ cells. **a** Soft agar colony formation assay. After stimulation by TGF-β in culture, cells were isolated by FACS and indicated numbers of cells were subjected to assay. **b** Formed colonies (*bar*, 500 μm). **c** Limiting dilution assay. The indicated numbers of CD13 + PLC liver cancer cells were inoculated into NOD/SCID mice. **d** The resultant tumor volumes

CSCs and liver CSCs have been reported.[21,33] To study the change of ROS status during EMT, intracellular ROS levels were measured by pro-oxidants using the 2′,7′-dichlorofluorescein diacetate (DCF-DA) stain. The data indicated that ROS level in $CD13^+$ cells was low compared with that in $CD13^-$ cells. ROS level of $CD13^+$/N-cadherin$^+$ cells was higher than that of $CD13^+$/N-cadherin$^-$ cells, suggesting that the TGF-β–induced EMT process is associated with an increase of ROS level (Fig. 4a). With regard to ROS scavengers in these cells, the qRT-PCR data indicated that the expression of *GCLM* and *GSS* was high in the $CD13^+$/N-cadherin$^-$ cells compared with the $CD13^-$/N-cadherin$^-$ cells (Fig. 4b). Interestingly, expression of *GCLM* and *GSS* was low in $CD13^+$/N-cadherin$^+$ cells compared with $CD13^+$/N-cadherin$^-$ cells (Fig. 4b), suggesting that TGF-β/EMT-induced ROS were metabolized to the appropriate level mainly via the CD13 function, rather than via the actions of the other scavengers, *GCLM* and *GSS*.

We speculated that the survival of TGF-β–induced EMT cells might be dependent on CD13 function. To confirm the involvement of ROS in TGF-β-induced EMT cells, cells were treated with the antioxidant *N*-acetylcysteine (NAC) in culture and measured resulting ROS level. By TGF-β treatment, expression of the N-cadherin, fibronectin, and vimentin was increased, but with NAC treatment, expression of N-cadherin and fibronectin was reduced (Fig. 4c). In contrast, expression of vimentin was increased by NAC with TGF-β treatment, suggesting that increased levels of ROS induce EMT, but should be controlled at suitable levels to sufficient induction of ROS.

To assess the effect of CD13 inhibition on TGF-β-induced EMT, cells were cultured in a medium containing ubenimex, which is an inhibitor of CD13. The data indicated that inhibition of CD13 by ubenimex elicited cell death and consequently suppressed N-cadherin in a dose-dependent manner (Fig. 4d). Additionally, as $CD13^+$ cells were enriched by TGF-β treatment, they were reduced by TGF-β with NAC treatment (Fig. 4e). We concluded that CD13 plays a role in the TGF-β-induced EMT properties of CD13 + liver cancer cells analyzed in the present study.

TGF-β-Induced CD13$^+$ Cells with Stem Cell Properties

We studied the expression of the stemness genes B lymphoma Mo-MLV insertion region 1 homolog (*BMI1*) and translocation-associated notch protein TAN-1 (*NOTCH1*). The data indicated that *BMI1* expression was significantly higher in $CD13^+$/N-cadherin$^+$ cells than in

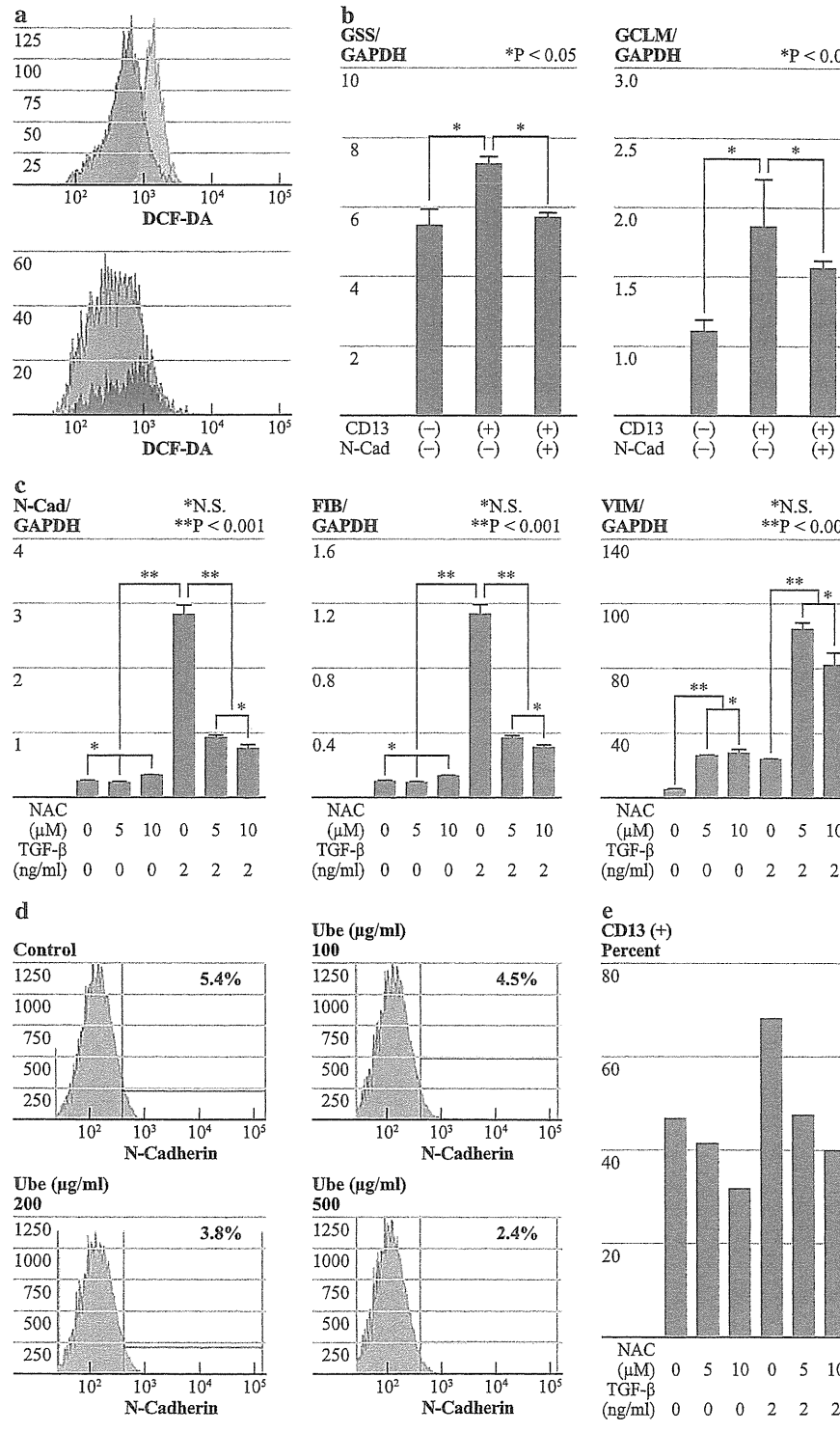

FIG. 4 TGF-β increase intracellular ROS level and induce EMT. **a** ROS level was measured after TGF-β exposure in culture. ROS level was detected by DCF-DA in the $CD13^+$, $CD13^-$, $CD13^+$N-cadherin$^-$, and $CD13^+$N-cadherin$^+$ fractions, as indicated. **b** qRT-PCR analysis of GSS and GCLM in $CD13^+$N-cadherin$^-$, $CD13^+$N-cadherin$^-$, and $CD13^+$N-cadherin$^+$ fractions. **c** Expression analysis of N-cadherin (N-cad), fibronectin (FIB), and vimentin (VIM) by qRT-PCR. Cells were treated by NAC with or without TGF-β in culture as indicated concentration. **d** Cells were cultured in medium containing ubenimex, an inhibitor of CD13, as indicated concentration and expression of N-cadherin was assessed. *Each number* indicates the percentage of N-cadherin expressing cells in each condition. **e** Expression of CD13 after treatment of NAC with or without TGF-β in culture as indicated concentration

$CD13^-$/N-cadherin$^-$ cells. Similarly, *NOTCH1* expression was significantly higher in $CD13^+$/N-cadherin$^+$ cells than in $CD13^+$/N-cadherin$^-$ cells, although expression in $CD13^+$/N-cadherin$^-$ cells was still significantly higher than that in $CD13^-$/N-cadherin$^-$ cells (Fig. 5a). Taken together that $CD13^+$/N-cadherin$^+$ cells have high tumorigenic ability next to $CD13^+$/N-cadherin$^-$ cells but express highest *BMI1* and *NOTCH1* expression, it can be thought that CD13+/N-cadherin + cells acquired stemness activity during EMT process induced by TGF-β.

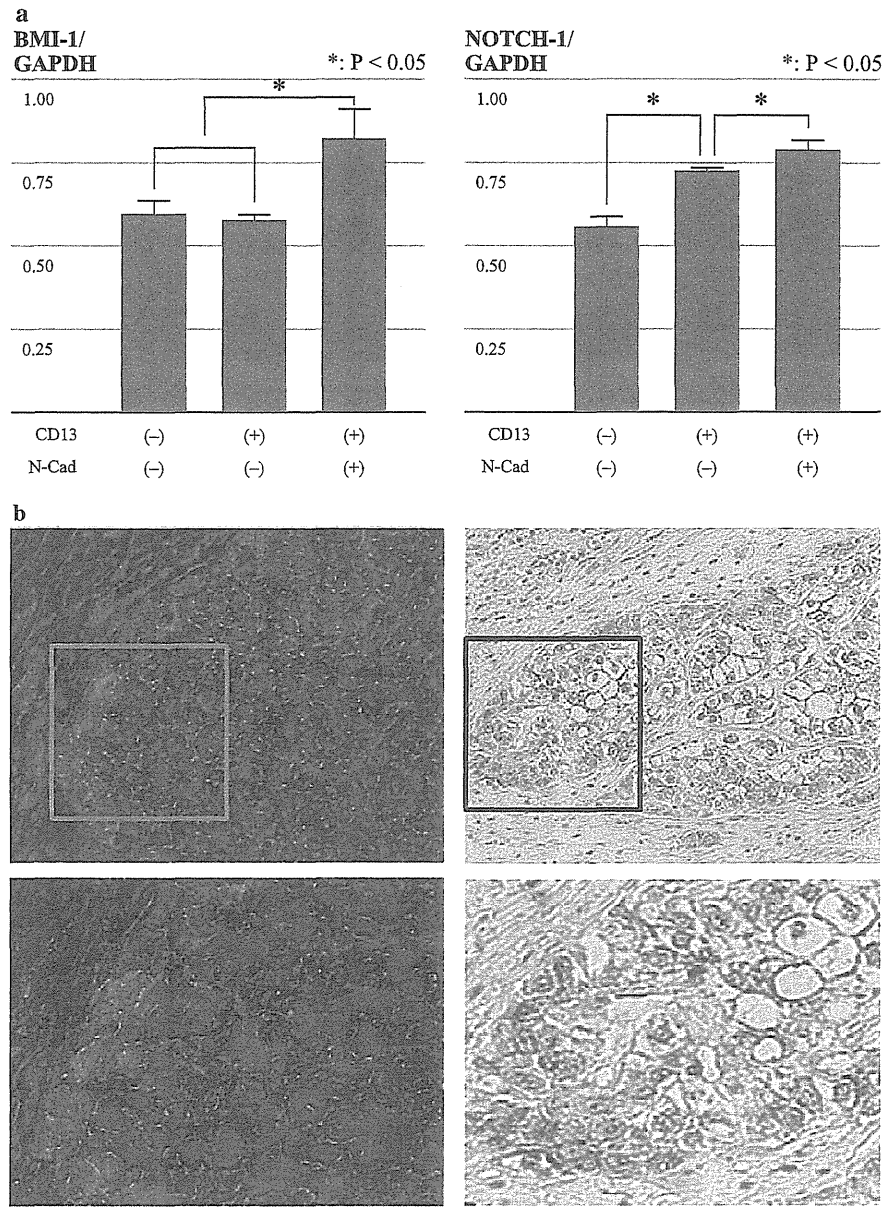

FIG. 5 CD13 and N-cadherin expression in human HCC sample. **a** Expression of BMI-1 and NOTCH1 in $CD13^{+}$N-$cadherin^{-}$, $CD13^{+}$N-$cadherin^{-}$, and $CD13^{+}$N-$cadherin^{+}$ fractions. After stimulation by TGF-β in culture, cells were isolated by FACS, RNA was extracted and qRT-PCR was performed. **b** Immunohistochemical analysis of post-TACE HCC sample stained with anti-human CD13 (*red*) and DAPI (*blue*) for the nucleus (*left*) and N-cadherin (*right*). *Lower panel* shows a higher magnification (×40) of the *square* in *upper column* (×10)

$CD13^{+}$/N-$cadherin^{+}$ Cells are Expressed in Therapy-Resistant HCC Cells

In the previous study, we have reported that CD13 + cells form cellular cluster along to fibrous capsule, especially after post-transcatheter arterial lipiodol chemoembolization (TACE) therapy.[21] To study N-cadherin expression in clinical hepatocellular carcinoma (HCC) sample, ten samples of HCC resected after TACE were used following study (Supplemental Table 1). Because CD13 was hard to detect in formalin-fixed sample, frozen sample was used to detect CD13 + cells. Our data indicated that, in all of the post-TACE samples examined, CD13 was found on the cell surface and N-cadherin expression was high (representative data shown in Fig. 5b). The surviving areas within the fibrous capsule of HCC tissue specimens taken after chemotherapy contained regions positive for both CD13 and N-cadherin; CD13 was expressed in adjacent regions of the HCC cells and formed bile canaliculi. Analysis of serial sections indicated that CD13 expression was combined with membrane expression of N-cadherin. The present data indicate that highly tumorigenic $CD13^{+}$/N-$cadherin^{+}$ HCC cells survive within the fibrous capsule of HCC tissues, suggesting that they are involved in therapy resistance and the aggressive behaviors of tumor cells after TACE.

DISCUSSION

Numerous reports have indicated that CSCs play a critical role in the generation of chemoradiation resistance.[1,2] Hence the findings that the EMT process could induce stemness in $CD24^+/CD44$ (low) CSC fractions in breast cancer, in $CD24^+/CD44^+/CD133^+$/Aldehyde Dehydrogenase$^+$ CSCs in pancreatic adenocarcinomas, and in $CD44^+/CD24^-$ CSCs in prostate cancer indicate a new epoch in cancer therapy.[27,34,35] Although our understanding of the link between therapy resistance, EMT, and metastasis remains unclear, in the present study, we show for the first time the functional relevance of CSC markers in the EMT phenomenon; our data suggest that in liver cancer, the functional CSC marker CD13 plays a role in the reduction of intracellular ROS, which has been shown to contribute to drug resistance.[21]

Emerging evidence supports the notion that EMT is an important step in tumor invasion and metastasis and is intimately involved in de novo and acquired chemoradiation resistance.[36] Consistent with this, the present data indicated that TGF-β exposure could induce the EMT phenotype but also elicit an increase in intracellular ROS and that this was reverted by the addition of a strong antioxidant (NAC) in culture. Recently, ROS have been found to be associated with tumor metastasis via tumor cell migration, invasion, and angiogenesis.[36] Thus, our findings suggest that strong chemopreventive agents antagonizing ROS could be useful for targeted reversal of EMT, which could become a novel approach for the prevention of tumor progression and metastasis. However, this type of inhibition would not kill CSCs but just suppress the cells. We also noted that an acute blockade of CD13, a natural, mild scavenger of intracellular ROS, in CD13-dependent malignant CSCs resulted in the induction of apoptosis,[21] suggesting the possible elimination of deleterious clones. The data suggest that a situation could arise wherein CSCs become accustomed to a relatively high level of intracellular ROS and are dependent on CD13 expression for the regulation of ROS levels; they survive by avoiding apoptosis. Thus, combining conventional chemotherapies, such as proliferation antagonizing 5-FU, with CSC-targeted reagents, such as ubenimex, may be beneficial for efficient tumor elimination.

Although simultaneous administration of 5-FU and ubenimex has been reported to have a synergic effect on tumor growth, the biological function of CD13 in liver CSCs remains to be elucidated.[21] To study the effect of CD13 inhibition on TGF-β-induced EMT, we cultured cells in a medium containing ubenimex, an inhibitor of CD13. Our data indicate that inhibition of CD13 by ubenimex elicited cell death and consequently resulted in dose-dependent suppression of N-cadherin, suggesting that CD13 plays a role in TGF-β-induced EMT properties in the $CD13^+$ liver cancer cells.

As biosynthesis, our data indicate that TGF-β stimulation elicits N-cadherin expression (EMT) as well as CD13 expression, presumably via the involvement of glycolysis and oxidative stress-responsive transcription factor c-Maf upstream of the CD13 gene's promoter (MAF-recognition element, MARE; Supplemental Fig. 1a and b), indicating that in the microenvironment of heterogeneous tumors, hypoxic conditions could increase the secretion of cytokines, such as IL6 and TGF-β from mesenchymal cells.[37,38] In cancer cells, these stimulate the response of Stat3 and hypoxia-inducible factors (HIFs) downstream of IL6 and of Smad4 downstream of TGF-β.[38] These in turn are involved in the transcriptional regulation of the proto-oncogene *c-MAF*, presumably via p300/CEBPbeta, AP1, and nuclear factor (NF) kappa B sites in its gene promoter.[38–41] Consequently, the present study proposes a natural working hypothesis where the hypoxic and inflammatory conditions in the microenvironment elicit cellular responses to increased CD13 expression that are beneficial for the survival of EMT-stimulated CSCs.

Although the majority of the experiments in this study are based on cell lines, the expression and ROS analyses support the contention that PLC cells reflect clinical HCC and may hold promise for preclinical studies. This study also suggests that the future development of liver cancer therapy based on CSC and EMT concepts appears promising. We are undertaking further analyses of clinical HCC samples to provide the necessary confirmation of our contention using in vivo assays.

ACKNOWLEDGMENT This study was supported in part by a grant from Core Research for Evolutional Science and Technology (CREST), a Grant-in-Aid for scientific research on Priority Areas (20012039), Grants-in-Aid for scientific research S (21229015) and C (20590313) from the Ministry of Education, Culture, Sports, Science, and Technology, and a grant from the Tokyo Biochemical Research Foundation, Japan.

REFERENCES

1. Sagar J, Chaib B, Sales K, Winslet M, Seifalian A. Role of stem cells in cancer therapy and cancer stem cells: a review. *Cancer Cell Int.* 2007;4:7–9.
2. Reya T, Morrison SJ, Clarke MF, Weissman IL. Stem cells, cancer, and cancer stem cells. *Nature.* 2001;414(6859):105–11.
3. Tan BT, Park CY, Ailles LE, Weissman IL. The cancer stem cell hypothesis: a work in progress. *Lab Invest.* 2006;86(12):1203–7.
4. Wulf GG, Wang RY, Kuehnle I, et al. A leukemic stem cell with intrinsic drug efflux capacity in acute myeloid leukemia. *Blood.* 2001;98(4):1166–73.
5. Lapidot T, Sirard C, Vormoor J, et al. A cell initiating human acute myeloid leukaemia after transplantation into SCID mice. *Nature.* 1994;367(6464):645–8.

6. Bonnet D, Dick JE. Human acute leukemia is organized as a hierarchy that originates from a primitive hematopoietic cell. *Nat Med.* 1997;3(7):730–7.
7. Piccirillo SG, Reynolds BA, Zanetti N, et al. Bone morphogenetic proteins inhibit the tumorigenic potential of human brain tumour-initiating cells. *Nature.* 2006;444(7120):761–5.
8. Bao S, Wu Q, McLendon RE, et al. Glioma stem cells promote radioresistance by preferential activation of the DNA damage response. *Nature.* 2006;444(7120):756–60.
9. Prince ME, Sivanandan R, Kaczorowski A, et al. Identification of a subpopulation of cells with cancer stem cell properties in head and neck squamous cell carcinoma. *Proc Natl Acad Sci USA.* 2007;104(3):973–8.
10. Al-Hajj M, Wicha MS, Benito-Hernandez A, Morrison SJ, Clarke MF. Prospective identification of tumorigenic breast cancer cells. *Proc Natl Acad Sci USA.* 2003;100(7):3983–8.
11. Ricci-Vitiani L, Lombardi DG, Pilozzi E, et al. Identification and expansion of human colon-cancer-initiating cells. *Nature.* 2007;445(7123):111–5.
12. O'Brien CA, Pollett A, Gallinger S, Dick JE. A human colon cancer cell capable of initiating tumour growth in immunodeficient mice. *Nature.* 2007;445(7123):106–10.
13. Haraguchi N, Utsunomiya T, Inoue H, et al. Characterization of a side population of cancer cells from human gastrointestinal system. *Stem Cells.* 2006;24(3):506–13.
14. Chiba T, Kita K, Zheng YW, et al. Side population purified from hepatocellular carcinoma cells harbors cancer stem cell-like properties. *Hepatology.* 2006;44(1):240–51.
15. Ding W, Mouzaki M, You H, et al. CD133 + liver cancer stem cells from methionine adenosyl transferase 1A-deficient mice demonstrate resistance to transforming growth factor (TGF)-beta-induced apoptosis. *Hepatology.* 2009;49(4):1277–86.
16. Ma S, Chan KW, Hu L, et al. Identification and characterization of tumorigenic liver cancer stem/progenitor cells. *Gastroenterology.* 2007;132(7):2542–56.
17. Zhu Z, Hao X, Yan M, et al. Cancer stem/progenitor cells are highly enriched in CD133(+)CD44(+) population in hepatocellular carcinoma. *Int J Cancer.* 2010;126(9):2067–78.
18. Yang ZF, Ngai P, Ho DW, et al. Identification of local and circulating cancer stem cells in human liver cancer. *Hepatology.* 2008;47(3):919–28.
19. Yang ZF, Ho DW, Ng MN, et al. Significance of CD90 + cancer stem cells in human liver cancer. *Cancer Cell.* 2008;13(2):153–66.
20. Yamashita T, Ji J, Budhu A, et al. EpCAM-positive hepatocellular carcinoma cells are tumor-initiating cells with stem/progenitor cell features. *Gastroenterology.* 2009;136(3):1012–24.
21. Haraguchi N, Ishii H, Mimori K, et al. CD13 is a therapeutic target in human liver cancer stem cells. *J Clin Invest.* 2010;120(9):3326–39.
22. Menrad A, Speicher D, Wacker J, Herlyn M. Biochemical and functional characterization of aminopeptidase N expressed by human melanoma cells. *Cancer Res.* 1993;53(6):1450–5.
23. Pasqualini R, Koivunen E, Kain R, et al. Aminopeptidase N is a receptor for tumor-homing peptides and a target for inhibiting angiogenesis. *Cancer Res.* 2000;60(3):722–7.
24. Mishima Y, Matsumoto-Mishima Y, Terui Y, et al. Leukemic cell-surface CD13/aminopeptidase N and resistance to apoptosis mediated by endothelial cells. *J Natl Cancer Inst.* 2002;94(13):1020–8.
25. Thiery JP, Acloque H, Huang RY, Nieto MA. Epithelial-mesenchymal transitions in development and disease. *Cell.* 2009;139(5):871–90.
26. Yang J, Weinberg RA. Epithelial-mesenchymal transition: at the crossroads of development and tumor metastasis. *Dev Cell.* 2008;14(6):818–29.
27. Mani SA, Guo W, Liao MJ, et al. The epithelial-mesenchymal transition generates cells with properties of stem cells. *Cell.* 2008;133(4):704–15.
28. Wu WS. The signaling mechanism of ROS in tumor progression. *Cancer Metastasis Rev.* 2006;25(4):695–705.
29. Radisky DC, Levy DD, Littlepage LE, et al. Rac1b and reactive oxygen species mediate MMP-3-induced EMT and genomic instability. *Nature.* 2005;436(7047):123–7.
30. Rees JR, Onwuegbusi BA, Save VE, Alderson D, Fitzgerald RC. In vivo and in vitro evidence for transforming growth factor-beta1-mediated epithelial to mesenchymal transition in esophageal adenocarcinoma. *Cancer Res.* 2006;66(19):9583–90.
31. Ito K, Hirao A, Arai F, et al. Regulation of oxidative stress by ATM is required for self-renewal of haematopoietic stem cells. *Nature.* 2004;431(7011):997–1002.
32. Ito K, Hirao A, Arai F, et al. Reactive oxygen species act through p38 MAPK to limit the lifespan of hematopoietic stem cells. *Nat Med.* 2006;12(4):446–51.
33. Diehn M, Cho RW, Lobo NA, et al. Association of reactive oxygen species levels and radioresistance in cancer stem cells. *Nature.* 2009;458(7239):780–3.
34. Dembinski JL, Krauss S. Characterization and functional analysis of a slow cycling stem cell-like subpopulation in pancreas adenocarcinoma. *Clin Exp Metastasis.* 2009;26(7):611–23.
35. Klarmann GJ, Hurt EM, Mathews LA, et al. Invasive prostate cancer cells are tumor initiating cells that have a stem cell-like genomic signature. *Clin Exp Metastasis.* 2009;26(5):433–46.
36. Wang Z, Li Y, Sarkar FH. Signaling mechanism(s) of reactive oxygen species in epithelial–mesenchymal transition reminiscent of cancer stem cells in tumor progression. *Curr Stem Cell Res Ther.* 2010;5(1):74–80.
37. Mahoney KM, Petrovic N, Schacke W, Shapiro LH. CD13/APN transcription is regulated by the proto-oncogene c-Maf via an atypical response element. *Gene.* 2007;403(1–2):178–87.
38. Nilsson CL, Dillon R, Devakumar A, et al. Quantitative phosphoproteomic analysis of the STAT3/IL-6/HIF1alpha signaling network: an initial study in GSC11 glioblastoma stem cells. *J Proteome Res.* 2010;9(1):430–43.
39. Kataoka K. Multiple mechanisms and functions of Maf transcription factors in the regulation of tissue-specific genes. *J Biochem.* 2007;141(6):775–81.
40. Cvekl A, Yang Y, Chauhan BK, Cveklova K. Regulation of gene expression by Pax6 in ocular cells: a case of tissue-preferred expression of crystalines in lens. *Int J Dev Biol.* 2004;48(8–9):829–44.
41. Hiramatsu Y, Suto A, Kashiwakuma D, et al. c-Maf activates the promoter and enhancer of the IL-21 gene, and TGF-b inhibits c-Maf-induced IL-21 production in CD4+T cells. *J Leukoc Biol.* 2010;87(4):703–12.

Published OnlineFirst March 27, 2012; DOI:10.1158/1078-0432.CCR-11-1078

Clinical Cancer Research

Microarray Analysis of Colorectal Cancer Stromal Tissue Reveals Upregulation of Two Oncogenic miRNA Clusters

Naohiro Nishida[1,4], Makoto Nagahara[2], Tetsuya Sato[3], Koshi Mimori[1], Tomoya Sudo[1], Fumiaki Tanaka[1], Kohei Shibata[1], Hideshi Ishii[1,4], Kenichi Sugihara[2], Yuichiro Doki[4], and Masaki Mori[1,4]

Abstract

Purpose: Cancer stroma plays an important role in the progression of cancer. Although alterations in miRNA expression have been explored in various kinds of cancers, the expression of miRNAs in cancer stroma has not been explored in detail.

Experimental Design: Using a laser microdissection technique, we collected RNA samples specific for epithelium or stroma from 13 colorectal cancer tissues and four normal tissues, and miRNA microarray and gene expression microarray were carried out. The expression status of miRNAs was confirmed by reverse transcriptase PCR. Furthermore, we investigated whether miRNA expression status in stromal tissue could influence the clinicopathologic factors.

Results: Oncogenic miRNAs, including two miRNA clusters, *miR-17-92a* and *miR-106b-25* cluster, were upregulated in cancer stromal tissues compared with normal stroma. Gene expression profiles from cDNA microarray analyses of the same stromal tissue samples revealed that putative targets of these miRNA clusters, predicted by Target Scan, such as *TGFBR2*, *SMAD2*, and *BMP* family genes, were significantly downregulated in cancer stromal tissue. Downregulated putative targets were also found to be involved in cytokine interaction and cellular adhesion. Importantly, expression of miR-25 and miR-92a in stromal tissues was associated with a variety of clinicopathologic factors.

Conclusions: Oncogenic miRNAs were highly expressed in cancer stroma. Although further validation is required, the finding that stromal miRNA expression levels were associated with clinicopathologic factors suggests the possibility that miRNAs in cancer stroma are crucially involved in cancer progression. *Clin Cancer Res; 18(11); 3054–70. ©2012 AACR.*

Introduction

Cancer tissues consist of cancer cells and surrounding stromal cells, including inflammatory cells, immunocompetent cells, endothelial cells, and fibroblasts. Cancer stroma interacts with cancer tissues directly or indirectly through cytokines, creating a niche for the cancer cells. Recent studies have focused on altered expression of oncogenes and tumor suppressor genes in stromal tissues. Kurose and colleagues reported that the downregulation of PTEN and p53 is a key step in breast cancer progression, and other reports have indicated that ablation of TGFBR2 in fibroblasts can lead to carcinogenesis *in vivo* (1–3).

With regard to clinical aspects, a number of studies have revealed the gene expression status of cancer stroma and its correlation to prognosis as well as clinicopathologic factors (4, 5). Particularly, Finak and colleagues analyzed global gene expression patterns in breast cancer stromal tissues and identified gene sets that potently influenced prognosis (6). They revealed that the aggressiveness of cancer could be defined by gene expression patterns in stromal tissue. Moreover, Fukino and colleagues revealed that cancer-specific LOH or allelic imbalance in stromal cells is more highly correlated with clinicopathologic features than that in epithelial cells (7). These findings suggest that cancer stromal tissues are actively involved in cancer progression.

miRNAs constitute a class of small (19–25 nucleotides) noncoding RNAs that function as posttranscriptional gene regulators by binding to their target mRNAs (8). Alterations in miRNA expression are reported in various kinds of human cancers, suggesting miRNAs function both as tumor suppressors and oncogenes in cancer development (9). Genetic alterations in cancer tissues are likely dependent largely on the expression status of miRNAs (9). We

Authors' Affiliations: [1]Department of Surgery and Molecular Oncology, Medical Institute of Bioregulation, Kyushu University, Oita; [2]Department of Surgical Oncology, Tokyo Medical and Dental University, Graduate School of Medical & Dental Science, Tokyo; [3]Center for Genomic Medicine, Kyoto University Graduate School of Medicine, Kyoto; and [4]Department of Gastroenterological Surgery, Osaka University Graduate School of Medicine, Osaka, Japan

Note: Supplementary data for this article are available at Clinical Cancer Research Online (http://clincancerres.aacrjournals.org/).

Corresponding Author: Masaki Mori, Department of Gastroenterological Surgery, Osaka University Graduate School of Medicine, 2-2 Yamada-oka, Suita City, Osaka 565-0871, Japan. Phone: 81-6-6879-3251; Fax: 81-6-6879-3259; E-mail: mmori@gesurg.med.osaka-u.ac.jp

doi: 10.1158/1078-0432.CCR-11-1078

Published OnlineFirst March 27, 2012; DOI:10.1158/1078-0432.CCR-11-1078

Translational Relevance

Cancer stroma plays a critical role in cancer progression. To investigate the role of miRNAs in colorectal cancer stroma, we carried out epithelial and stromal tissue-specific miRNA microarray analyses using a laser microdissection technique. We found that oncogenic miRNAs, including the *miR-17-92a* cluster and the *miR-106b-25* cluster, which are known to be involved in cancer progression in epithelial tissue, were significantly upregulated in cancer stromal tissue compared with normal stroma. Gene expression profiles from cDNA microarray analyses of the same stromal tissue samples revealed that putative targets of these miRNA clusters, predicted by TargetScan, such as *TGFBR2*, *SMAD2*, and *BMP* family genes, were significantly downregulated in cancer stromal tissue. Furthermore, miRNA expression in colorectal cancer stroma was associated with a number of clinicopathologic factors. Although further validation is required, these findings suggest the possibility that miRNAs in stromal tissues are functionally associated with cancer progression.

considered the possibility that gene expression in cancer stroma is also regulated by miRNAs expressed in cancer stroma.

Conventional gene expression analysis using bulk tumor samples could not reveal the gene and miRNA expression profiles in cancer stroma. In this study, using a laser microdissection (LMD) method, we collected epithelium-specific and stoma-specific RNAs, and investigated the miRNA and gene expression profiles. By analyzing many kinds of microarray data, including that of epithelium, stroma, normal, and cancer, we show how miRNAs in cancer stroma are involved in cancer progression.

Materials and Methods

Clinical samples

Tissues from 13 cases of colorectal cancer and 4 normal colorectal tissues (located more than 5 cm from the colorectal cancer) were obtained during surgery. All patients underwent resection of the primary tumor at Kyushu University Hospital at Beppu and affiliated hospitals between 1993 and 2006. Written informed consent was obtained from all patients, and the study protocol was approved by the local ethics committee. Detailed information is described in Supplementary Data.

Laser microdissection

Tissue samples were microdissected using the LMD system LMD6000 (Leica Laser Microdissection System; Leica Microsystems) as previously described (10). Detailed protocols are described in Supplementary Information.

To show the accuracy of LMD and RNA separation, we presented tissue section before (left) and after (right) LMD in 6 representative samples of colorectal cancer (Supplementary Fig. S1).

miRNA microarray

Total RNAs from epithelial and stromal tissues of cancer and normal samples were analyzed by miRNA microarray. Total RNA was extracted from tissue using the miRNeasy Mini Kit (Qiagen) according to the manufacturer's protocol. Concentrations and purities of the total RNAs were assessed with a spectrophotometer and RNA integrity was verified using an Agilent 2100 Bioanalyzer (Agilent Technologies). OD_{260}/OD_{280} ratios of 1.8 to 2.1 were accepted to be adequate for microarray. Total RNA (100 ng) was directly labeled with cyanine 3-CTP (Cy3), without fractionation or amplification, using an Agilent protocol that produces precise and accurate measurements spanning a linear dynamic range from 0.2 amol to 2 fmol of input miRNA. Each total RNA sample (100 ng) was competitively hybridized to a miRNA array (Agilent Microarray Design ID = 014947, Early Access version) containing 455 miRNAs [version 15 of the Sanger miRNA database (http://www.mirbase.org/)], according to the manufacturer's protocol (11). The intensity of each hybridization signal was evaluated using Extraction Software Version A.7.5.1 (Agilent Technologies), which used the locally weighted linear regression curve fit (LOWESS) normalization method (12).The robust multiarray average algorithm normalization method was also used for analysis in downregulated miRNAs in cancer stroma (13, 14). miRNA arrays have been deposited in the National Center for Biotechnology Information (NCBI) Gene Expression Omnibus (GEO) database with accession code GSE35602.

cDNA microarray

We used the commercially available Human Whole Genome Oligo DNA Microarray Kit (Agilent Technologies). A list of genes on this cDNA microarray is available from http://www.chem.agilent.com. Cyanine (Cy)-labeled cRNA was prepared using T7 linear amplification as described in the Agilent Low RNA Input Fluorescent Linear Amplification Kit Manual (Agilent Technologies). Labeled cRNA was fragmented and hybridized to an oligonucleotide microarray (Whole Human Genome 4 × 44 K Agilent G4112F). Fluorescence intensities were determined with an Agilent DNA Microarray Scanner and were analyzed using G2567AA Feature Extraction Software Version A.7.5.1 (Agilent Technologies), which used the LOWESS normalization method (12). This microarray study followed MIAME guidelines issued by the Microarray Gene Expression Data group (15). Gene expression arrays have been deposited in the NCBI GEO database with accession code GSE35602.

Gene ontology analysis and miRNA target prediction

A total of 1,939 Gene set enrichment analyses of differentially expressed genes were carried out using Gene Codis version 2.0 (16, 17). The Kyoto Encyclopedia of Genes and

Published OnlineFirst March 27, 2012; DOI:10.1158/1078-0432.CCR-11-1078

Genomes (KEGG) database (18) was used for systematic analysis of gene functions. TargetScan (19, 20) Version 5.1 algorithm was used to predict putative targets of each miRNA. TargetScan focuses on the exact match to 7 bases or more (hexamer match in positions 2–7, plus an adenosine at a position on the 3′ side) of the miRNA seed sequence in the 3′-untranslated region of target messenger RNA. In our analysis, we included all targets that met TargetScan criteria without taking into account evolutionary conservation.

Quantitative real-time reverse transcriptase PCR

For *miR-25* and *miR-92a* quantitative real-time reverse transcriptase PCR (qRT-PCR), cDNA was synthesized from 10 ng of total RNA using TaqMan miRNA hsa-*miR-25*- or *92a*-specific primers (Applied Biosystems) and a TaqMan MicroRNA Reverse Transcription Kit (Applied Biosystems). RT-PCR protocols are described in Supplementary Information.

Statistical analysis

Differences between groups were estimated using the χ^2 test and Student *t* test. After expression signals were calculated by $\log_2$ transformation of the normalized data, differentially expressed miRNAs and genes were detected by using the fold-change value and *Q* value. We used the significance analysis of microarrays method in the "samr" package of the R language (http://www.r-project.org/). RT-PCR data were analyzed using JMP software (SAS Institute Inc.). All differences were considered statistically significant at the level of $P < 0.05$ or $Q < 0.05$.

Results

The miR-17-92a cluster and miR-106b-25 cluster were upregulated in cancer stroma compared with normal stroma

To investigate the functions of miRNAs in cancer stroma, we carried out miRNA microarray analyses with samples of 13 cancer stromal tissue and 4 samples of normal stromal tissue. Those miRNAs that were significantly upregulated in cancer stromal tissues compared with normal stromal tissues are listed in Table 1 (fold change >1.5, and $Q < 0.05$). For example, oncogenic miRNAs, including *miR-21*, *miR-221*, and almost all components of the oncogenic *miR-17-92a* cluster and *miR-106b-25* cluster except *miR-19b* were upregulated in cancer stromal tissue compared with normal stromal tissue (Table 1). Unsupervised hierarchical clustering of normal and cancerous stromal samples revealed that all components of the *miR-17-92a* cluster and the *miR-106b-25* cluster (except for *miR-92a*) were classified in the same cluster (Supplementary Fig. S2A and S2B). *MiR-92a* was classified in another cluster, perhaps because *miR-92a* has a homolog (*miR-92a-2*) on chromosome X, besides *miR-92a-1* in the miRNA cluster on chromosome 13 (21). Therefore, its expression could have diverged from the expression of other miRNAs in the cluster.

The correlation coefficient ratio was significantly higher within miRNA clusters (Supplementary Table S1). These clusters are transcribed from another chromosome. The *miR-17-92a* cluster was located on chromosome 13 in the host gene *C13ORF25*, and its homolog *miR-106b-25* cluster was located in the intron of the host gene MCM7 on chromosome 7 (Fig. 1, top part). Some components shared the same seed sequence (Fig. 1, bottom part), suggesting they regulated the same targets simultaneously.

In 4 of the 13 samples of cancer tissue and the 4 normal tissues, both epithelial and stromal samples were available. Thus, we carried out combined analyses in epithelial and stromal tissues in these samples. The expression status of epithelial tissues was highly correlated with that of stromal tissues, and the expression of miRNA in the epithelium was always higher than that in the stroma in all components of the *miR-17-92a* cluster and the *miR-106b-25* cluster (Fig. 2).

Significantly downregulated genes which are putative targets of the miR-17-92a and miR-106b-25 clusters are involved in a variety of cellular functions

We also carried out gene expression array analyses using the same samples used in the miRNA microarray. We identified significantly downregulated genes (fold change < 0.5 and $Q < 0.05$), which were putative targets of the *miR-17-92a* and *miR-106b-25* clusters. The number of genes that matched these criteria was 1,939. Gene set enrichment analysis using Gene Codis version 2.0 (16, 17) and KEGG revealed that the following molecules were enriched: KEGG 04060: cytokine–cytokine receptor interaction [chemokines, hematopoietins, platelet-derived growth factor (PDGF) family, TNF family, and TGFβ family], KEGG 04340: hedgehog signaling pathway, KEGG 05200: pathways in cancer, and KEGG 04514: cell adhesion molecules (CAM; Table 2, Supplementary Table S2A). These indicated the possibility that the *miR-17-92a* and *miR-25-106b* clusters were involved in those important pathways in colorectal cancer stroma.

Identification of a putative miRNA gene pathway focusing on inverse correlations between miRNAs and genes

We used different approaches to identify putative targets of the *miR-17-92a* and *miR-106b-25* clusters. Combining the microarray data of miRNAs and genes in stromal samples, we identified highly inversely correlated miRNA gene pairs, which were putative pathways predicted by TargetScan (refs. 19, 20; correlation coefficient >0.65 and $P < 0.05$; Table 3). These included a number of crucial regulators of cellular function, such as the apoptosis-related *miR-17* death-associated protein kinase 2 (*DAPK*) pairing, the *miR-18a*–caspase 7 pairing, and the *miR-17* cancer-related transcription factor 7 (*TCF7*) pairing.

miR-25 and miR-92a expression status in colorectal cancer stromal tissue

The miRNA array analysis revealed that 2 oncogenic miRNA clusters were upregulated in colorectal cancer stroma. Therefore, we confirmed the expression status of 2

Published OnlineFirst March 27, 2012; DOI:10.1158/1078-0432.CCR-11-1078

Table 1. Upregulated miRNAs in colorectal cancer stromal tissue compared with normal stromal tissue

Systematic name	Signal in cancer stromal tissue (log_2)	Signal in normal stromal tissue (log_2)	Fold change	*Q* (%)
hsa-miR-214	7.3612	5.1633	4.5882	0.0000
hsa-miR-21	13.7414	11.7651	3.9348	0.0000
hsa-miR-455-3p	5.0351	3.4322	3.0376	0.0000
hsa-miR-663	4.4278	2.7578	3.1820	0.0000
hsa-miR-127-3p	3.7355	1.9303	3.4947	0.0000
hsa-miR-92a	7.2865	5.7584	2.8842	0.0000
hsa-miR-381	3.9035	2.5478	2.5593	0.0000
hsa-miR-93	5.5042	4.0246	2.7886	0.0000
hsa-miR-224	4.5767	2.2308	5.0840	0.0000
hsa-miR-432	2.6401	1.3709	2.4102	0.0000
hsa-miR-221	5.1187	3.6628	2.7433	0.0000
hsa-miR-125b	7.7959	5.7433	4.1486	0.0000
hsa-miR-17	6.3813	4.9449	2.7064	0.0000
hsa-miR-337-5p	2.8150	1.4391	2.5952	0.0000
hsa-miR-502-3p	1.8047	0.5097	2.4538	0.0000
hsa-miR-300	3.6767	2.3557	2.4985	0.0000
hsa-miR-128	2.5359	1.3263	2.3127	0.0000
hsa-miR-532-5p	2.7469	1.5402	2.3080	0.0000
hsa-miR-609	3.8840	2.8980	1.9806	0.0000
hsa-miR-130b	4.1915	2.7904	2.6409	0.0000
hsa-miR-18a	3.7635	1.3688	5.2588	0.0000
hsa-miR-181d	3.1301	2.0477	2.1175	0.0000
hsa-miR-362-5p	3.2330	2.0853	2.2156	0.0000
hsa-miR-424	7.7230	5.9653	3.3816	0.0000
hsa-miR-152	3.1990	1.6066	3.0156	0.0000
hsa-miR-654-3p	4.3411	2.6129	3.3130	0.0000
hsa-miR-149	3.8869	2.7086	2.2632	0.0000
hsa-miR-7	4.7678	2.8344	3.8196	0.0000
hsa-miR-485-3p	5.3006	4.2385	2.0880	0.0000
hsa-miR-99b	3.9191	2.6203	2.4603	0.0000
hsa-miR-933	2.7300	1.7161	2.0193	0.0000
hsa-miR-615-3p	3.8335	2.6442	2.2804	0.0000
hsa-miR-640	2.9456	1.4328	2.8535	0.0000
hsa-miR-483-3p	6.2669	5.0075	2.3940	0.0000
hsa-miR-605	3.8121	2.5917	2.3301	0.0000
hsa-miR-135b	3.8255	0.7653	8.3408	0.0000
hsa-miR-296-5p	1.9389	1.1457	1.7329	0.0000
hsa-miR-647	3.8730	2.1903	3.2102	0.0000
hsa-miR-1236	3.4103	1.8925	2.8635	0.0000
hsa-miR-34b	4.2683	2.3956	3.6620	0.0000
hsa-miR-592	2.5548	0.8012	3.3721	0.4839
hsa-miR-25	5.9887	4.7911	2.2936	0.4839
hsa-let-7i	8.6952	7.6400	2.0781	0.4839
hsa-miR-20b	5.5041	4.2857	2.3269	0.4839
hsa-miR-130a	7.3585	6.0856	2.4165	0.4839
hsa-miR-199a-5p	7.4083	5.9666	2.7163	0.4839
hsa-miR-1238	4.2775	3.5734	1.6291	0.4839
hsa-miR-331-3p	6.6993	5.5074	2.2846	0.4839
hsa-miR-24	9.5984	8.5492	2.0693	0.4839
hsa-miR-20a	7.5321	6.3601	2.2532	0.4839
hsa-miR-23a	10.0837	9.0655	2.0254	0.4839
hsa-miR-199b-5p	6.7800	5.3520	2.6907	0.4839
hsa-miR-181b	4.6692	3.7467	1.8955	0.4839

(Continued on the following page)

Published OnlineFirst March 27, 2012; DOI:10.1158/1078-0432.CCR-11-1078

Table 1. Upregulated miRNAs in colorectal cancer stromal tissue compared with normal stromal tissue (Cont'd)

Systematic name	Signal in cancer stromal tissue (log_2)	Signal in normal stromal tissue (log_2)	Fold change	Q (%)
hsa-miR-377	4.4965	3.2165	2.4283	0.4839
hsa-miR-18b	2.5247	0.9391	3.0013	0.4839
hsa-miR-539	2.0809	1.0446	2.0510	0.4839
hsa-miR-22	9.7884	8.6262	2.2379	0.4839
hsa-miR-223	8.8473	7.7969	2.0712	0.4839
hsa-miR-491-3p	2.5471	0.9916	2.9393	0.4839
hsa-miR-125a-5p	5.6168	4.5834	2.0469	0.4839
hsa-miR-299-5p	3.1356	1.7790	2.5607	0.4839
hsa-miR-483-5p	4.9531	3.9757	1.9689	0.4839
hsa-miR-379	2.4551	0.4574	3.9938	0.4839
hsa-miR-1234	5.0701	4.3136	1.6894	0.4839
hsa-miR-99a	3.9888	2.3726	3.0657	0.4839
hsa-miR-1225-3p	3.9937	3.3510	1.5613	0.4839
hsa-miR-495	2.3389	0.7363	3.0369	0.4839
hsa-miR-574-5p	7.1083	6.2371	1.8292	0.4839
hsa-miR-125a-3p	3.2257	2.3094	1.8873	0.4839
hsa-miR-326	1.9496	0.8913	2.0825	0.4839
hsa-miR-1224-3p	4.8757	3.6868	2.2798	0.4839
hsa-miR-1229	3.7613	2.5318	2.3448	0.4839
hsa-miR-937	4.9785	3.8112	2.2459	0.4839
hsa-miR-574-3p	7.9370	7.0906	1.7979	0.4839
hsa-miR-1237	2.8475	2.0403	1.7498	0.4839
hsa-miR-206	3.0294	1.7743	2.3868	0.4839
hsa-miR-129-3p	1.7338	0.7030	2.0432	0.4839
hsa-miR-885-5p	6.2987	5.1769	2.1761	0.4839
hsa-miR-1227	4.6286	3.0407	3.0061	0.4839
hsa-miR-631	4.3710	2.9772	2.6277	0.4839
hsa-miR-487b	2.2864	0.5419	3.3507	0.8249
hsa-miR-543	1.4302	0.1764	2.3847	0.8249
hsa-miR-365	6.3121	5.3710	1.9200	0.8249
hsa-let-7e	6.8754	5.9369	1.9166	0.8249
hsa-miR-151-3p	3.8653	2.8896	1.9666	0.8249
hsa-miR-106b	6.7077	5.7538	1.9371	0.8249
hsa-miR-301a	4.3942	3.3753	2.0263	0.8249
hsa-miR-382	2.2284	0.8661	2.5709	0.8249
hsa-miR-100	4.7280	3.4939	2.3523	0.8249
hsa-miR-452	2.3510	1.1210	2.3456	0.8249
hsa-miR-371-5p	2.2495	1.1375	2.1614	0.8249
hsa-miR-765	4.3601	3.6031	1.6900	0.8249
hsa-miR-362-3p	2.5044	1.5707	1.9102	0.8249
hsa-miR-183	1.8260	0.5658	2.3953	0.8249
hsa-miR-423-5p	3.8130	3.0448	1.7032	0.8249
hsa-miR-328	6.1455	5.1186	2.0377	0.8249
hsa-miR-595	4.4023	3.3593	2.0605	0.8249
hsa-miR-542-3p	2.8903	1.2498	3.1177	0.8249
hsa-miR-550	1.9877	1.2773	1.6363	0.8249
hsa-miR-634	2.1901	1.4710	1.6462	0.8249
hsa-miR-188-5p	4.1637	3.5119	1.5711	1.3079
hsa-miR-450a	2.6452	1.0431	3.0358	1.3079
hsa-miR-181c	2.7493	1.7464	2.0040	1.3079
hsa-miR-126	8.1419	7.2671	1.8338	1.3079
hsa-miR-484	3.8659	3.2581	1.5239	1.3079

(Continued on the following page)

Published OnlineFirst March 27, 2012; DOI:10.1158/1078-0432.CCR-11-1078

Table 1. Upregulated miRNAs in colorectal cancer stromal tissue compared with normal stromal tissue (Cont'd)

Systematic name	Signal in cancer stromal tissue (log_2)	Signal in normal stromal tissue (log_2)	Fold change	*Q* (%)
hsa-miR-95	2.2341	1.4163	1.7627	1.3079
hsa-miR-19a	7.0755	6.2318	1.7946	1.3079
hsa-miR-181a	6.7619	5.9594	1.7441	1.3079
hsa-miR-376a	4.3021	3.2870	2.0211	1.3079
hsa-miR-425	4.4042	3.5379	1.8230	1.3079
hsa-miR-455-5p	1.9466	0.6533	2.4510	1.3079
hsa-miR-324-3p	5.1796	4.5422	1.5555	1.3079
hsa-miR-622	2.5718	1.6357	1.9133	1.3079
hsa-miR-613	1.6581	0.9437	1.6408	1.3079
hsa-miR-575	3.9488	3.2521	1.6208	1.3079
hsa-miR-222	3.2655	2.5148	1.6827	1.3079
hsa-miR-32	2.5684	1.6119	1.9406	1.3079
hsa-miR-197	7.9098	7.0983	1.7551	1.3079
hsa-miR-766	6.9197	6.0107	1.8777	1.3079
hsa-miR-876-5p	1.3810	0.6503	1.6595	1.9848
hsa-miR-505	2.8023	2.0524	1.6817	1.9848
hsa-let-7c	7.3815	6.6304	1.6831	1.9848
hsa-miR-98	4.5308	3.7445	1.7247	1.9848
hsa-miR-27a	9.1504	8.3246	1.7725	1.9848
hsa-miR-324-5p	4.1229	3.2487	1.8330	1.9848
hsa-miR-874	3.6715	3.0471	1.5416	1.9848
hsa-miR-133a	1.3162	0.6960	1.5371	1.9848

NOTE: miRNAs which are components of miR-17-92a cluster or miR-25-106b cluster are marked (gray).

representative miRNAs from the 2 clusters, *miR-25*, and *miR-92a* in clinical samples. *MiR-25* and *miR-92a* are selected because of relative high expression in cancer stroma and because they have the same seed sequence and share the same targets and could work coordinately. In samples of normal epithelial tissue ($n = 4$), cancer epithelial tissue ($n = 10$), normal stromal tissue ($n = 4$), and cancer stromal tissue ($n = 26$), which included 13 cancer samples and 4

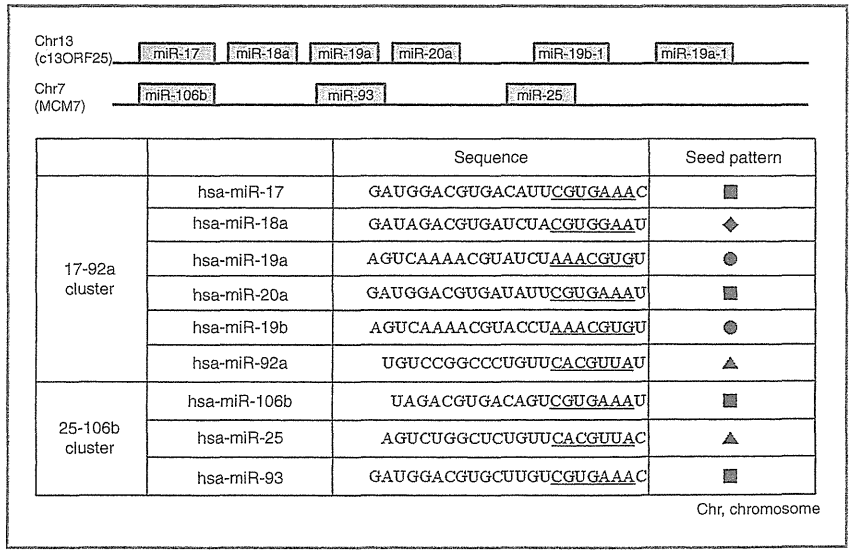

Figure 1. Top, schematic diagram showing the genomic structures of the 2 miRNA clusters located on chromosomes 13 and 7. The *miR-17-92a* cluster is located in the intron of host gene *C13ORF25* and *miR-25-106b* is in *MCM7*. Bottom, sequences of 2 miRNA cluster components. The same marks indicate seed sequence (2–8 mer from the 5′side) homology between the individual miRNAs.

Published OnlineFirst March 27, 2012; DOI:10.1158/1078-0432.CCR-11-1078

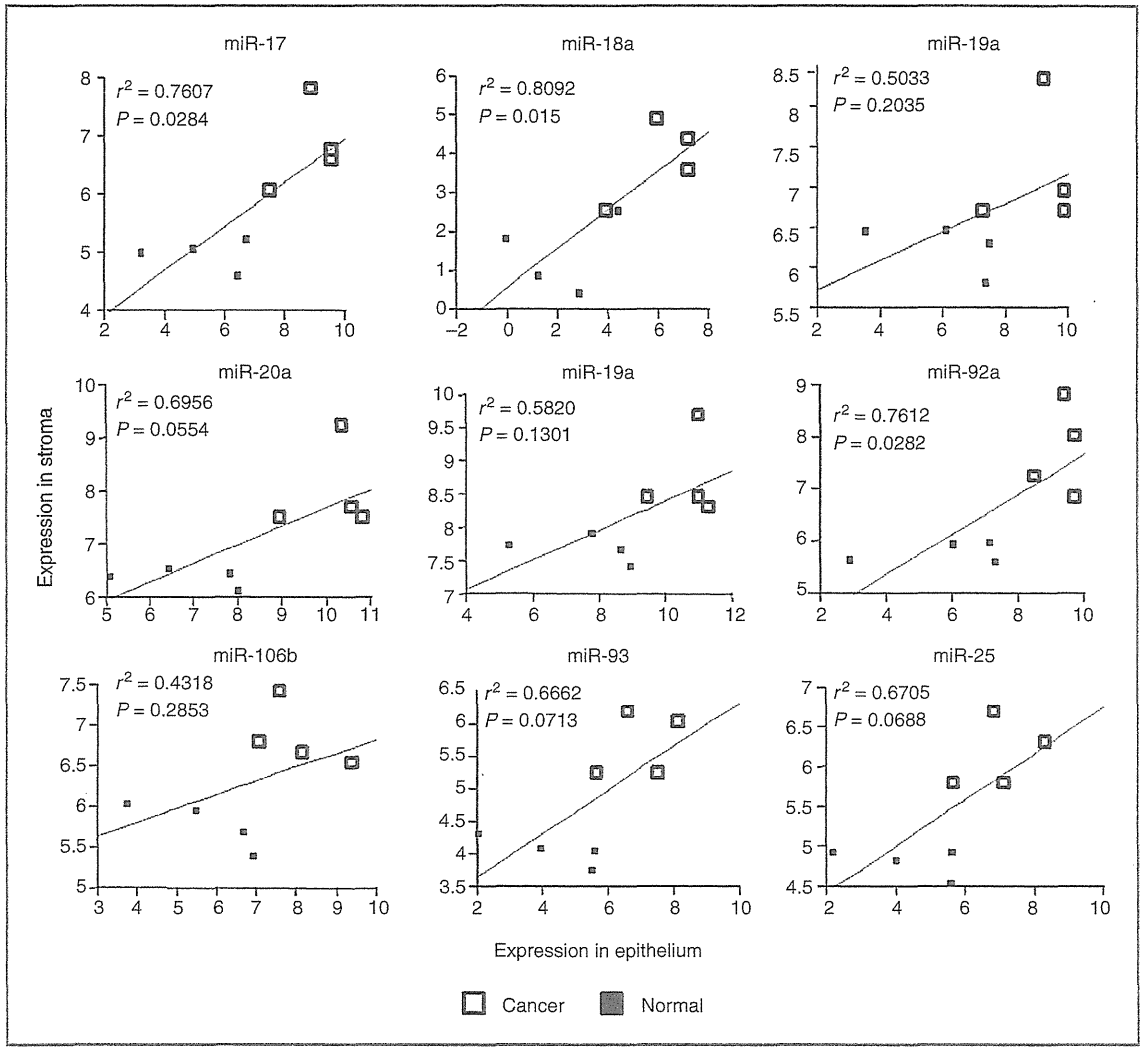

Figure 2. Correlation between the expression status of epithelial tissue and stromal tissue of *miR-17-92a* and *miR-25-106b* clusters. In all components of the clusters, expression status of the epithelial tissues and the stromal tissues was highly correlated and expression was higher in epithelium than in stroma.

normal samples used for microarray analysis, we carried out qRT-PCR to investigate the expression of *miR-25* and *miR-92a*. The data confirmed the upregulation of these miRNAs in cancer stroma compared with normal stroma in accordance with upregulation in cancer epithelium (Fig. 3).

miR-25 and miR-92a expression in colorectal cancer stroma was associated with clinicopathologic factors

For the 26 colorectal cancer stromal samples for which we used RT-PCR analysis, clinicopathologic data were available in 24 cases. Clinicopathologic analysis revealed that the high *miR-25* expression group (values > the 0.25 quartile; 0.54, normalized to RNU6B) had more advanced venous invasion compared with the low expression group (values < the 0.25 quartile; $P = 0.046$, Table 4). In the high *miR-92a* expression group (values > the 0.75 quartile; 1.16, normalized to RNU6B), there was greater lymphatic invasion ($P = 0.005$), venous invasion ($P = 0.016$), and liver metastasis ($P = 0.018$) compared with the low *miR-92a* expression group (values < the 0.75 quartile; Table 5). However, no significant differences were observed regarding age, gender, histology, lymphatic invasion, venous invasion, lymph node metastasis, peritoneal dissemination, or distant metastasis.

Downregulated miRNAs in colorectal cancer stromal tissue compared with normal stromal tissue

We also investigated downregulated miRNAs in cancer stroma compared with normal stroma. As a result,

Published OnlineFirst March 27, 2012; DOI:10.1158/1078-0432.CCR-11-1078

Table 2. Genes downregulated in cancer stroma, which are putative targets of miR-17-92a and/or miR-25-106b clusters

Gene symbol	Genbank accession	Description	Fold Change[a]	Q (%)[a]	miR-17/20a/ 106b/93 target[b]	miR-18a target[b]	miR-19a/ 19b target[b]	miR-92a/25 target[b]
KEGG 04061: Cytokine–cytokine receptor interaction (chemokines, hematopoietins, PDGF family, TNF family, and TGFβ family)								
IL10RA	NM_001558	*Homo sapiens* interleukin 10 receptor, α (IL10RA)	0.2492	0.0000	○	○	○	
TNFRSF17	NM_001192	*Homo sapiens* TNF receptor superfamily, member 17 (TNFRSF17)	0.1313	0.0000	○	○		
LIFR	NM_002310	*Homo sapiens* leukemia inhibitory factor receptor alpha (LIFR)	0.1563	0.0000	○	○	○	
CXCL12	NM_199168	*Homo sapiens* chemokine (C-X-C motif) ligand 12 (stromal cell–derived factor 1; CXCL12), transcript variant 1	0.1218	0.0000			○	
BMP2	NM_001200	*Homo sapiens* bone morphogenetic protein 2 (BMP2)	0.1734	0.0748	○	○		
CNTFR	NM_147164	*Homo sapiens* ciliary neurotrophic factor receptor (CNTFR), transcript variant 1	0.2142	0.0748			○	
IL6R	NM_000565	*Homo sapiens* interleukin 6 receptor (IL6R), transcript variant 1	0.2694	0.0748	○	○		
PDGFRA	BC015186	*Homo sapiens* platelet-derived growth factor receptor, α polypeptide, mRNA (cDNA clone IMAGE: 4043984), complete cds.	0.2247	0.1256	○			○
TNFRSF13B	NM_012452	*Homo sapiens* TNF receptor superfamily, member 13B (TNFRSF13B)	0.2033	0.1256				○
XCL1	NM_002995	*Homo sapiens* chemokine (C motif) ligand 1 (XCL1)	0.1676	0.1256	○	○	○	○
CTF1	NM_001330	*Homo sapiens* cardiotrophin 1 (CTF1)	0.3178	0.2025		○		
XCL2	NM_003175	*Homo sapiens* chemokine (C motif) ligand 2 (XCL2)	0.2028	0.2025	○	○	○	
CCR9	NM_006641	*Homo sapiens* chemokine (C-C motif) receptor 9 (CCR9), transcript variant B	0.2514	0.2025	○	○	○	○
TGFBR2	NM_003242	*Homo sapiens* TGF, β receptor II (70/80 kDa) (TGFBR2), transcript variant 2	0.3819	0.3097	○		○	
CCL16	NM_004590	*Homo sapiens* chemokine (C-C motif) ligand 16 (CCL16)	0.3502	0.4833				○
IFNA2	NM_000605	*Homo sapiens* IFN, α 2 (IFNA2)	0.4167	0.7799		○	○	
GHR	NM_000163	*Homo sapiens* growth hormone receptor (GHR)	0.3538	0.7799			○	○
IFNW1	NM_002177	*Homo sapiens* IFN, omega 1 (IFNW1)	0.3926	0.7799			○	
IL15	NM_172174	*Homo sapiens* interleukin 15 (IL15), transcript variant 1	0.4331	0.7799				○
LEP	NM_000230	*Homo sapiens* leptin (obesity homolog, mouse; LEP)	0.3591	0.7799	○			
BMPR1B	NM_001203	*Homo sapiens* bone morphogenetic protein receptor, type IB (BMPR1B)	0.4251	1.2419	○	○		
FASLG	NM_000639	*Homo sapiens* Fas ligand (TNF superfamily, member 6; FASLG)	0.4284	1.2419	○	○	○	○

(Continued on the following page)